

Large Field-of-View Nonlinear Holography in Lithium Niobate

Xiaoyi Xu,[§] Pengcheng Chen,[§] Taxue Ma,[§] Jianan Ma, Chao Zhou, Yawen Su, Mingxin Lv, Weiwen Fan, Bohan Zhai, Yuyang Sun, Tianxin Wang, Xiaopeng Hu, Shi-Ning Zhu, Min Xiao, and Yong Zhang^{*}



Cite This: *Nano Lett.* 2024, 24, 1303–1308



Read Online

ACCESS |

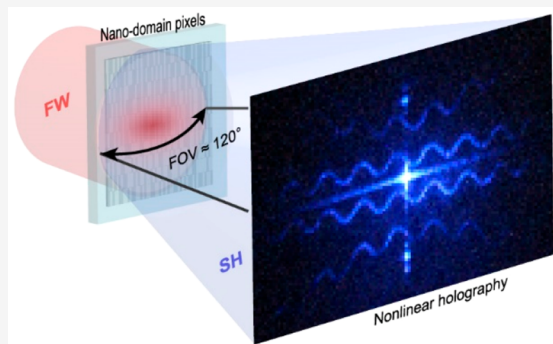
Metrics & More

Article Recommendations

Supporting Information

ABSTRACT: A nonlinear holographic technique is capable of processing optical information in the newly generated optical frequencies, enabling fascinating functions in laser display, security storage, and image recognition. One popular nonlinear hologram is based on a periodically poled lithium niobate (LN) crystal. However, due to the limitations of traditional fabrication techniques, the pixel size of the LN hologram is typically several micrometers, resulting in a limited field-of-view (FOV) of several degrees. Here, we experimentally demonstrate an ultra-high-resolution LN hologram by using the laser poling technique. The minimal pixel size reaches 200 nm, and the FOV is extended above 120° in our experiments. The image distortions at large view angles are effectively suppressed through the Fourier transform. The FOV is further improved by combining multiple diffraction orders of SH fields. The ultimate FOV under our configuration is decided by a Fresnel transmission. Our results pave the way for expanding the applications of nonlinear holography to wide-view imaging and display.

KEYWORDS: nonlinear holography, large field-of-view, lithium niobate, nanodomain engineering, femtosecond laser direct writing



Optical holography has been widely applied in optical display, data storage,^{1,2} information security,^{3–5} and microscopy⁶ since its invention.⁷ This method is capable of reconstructing both the intensity and phase information on an object in a light field. With the rapid development of computer technology, computer-generated holograms (CGHs) have attracted more research interest, which can be feasibly realized by spatial light modulators (SLMs).^{8–10} However, the popular liquid-crystal-based SLM features a typical pixel pitch of tens of micrometers, which severely limits the quality of the reconstructed field, including the field-of-view (FOV). Here, the FOV is defined by the equation $\theta = 2 \sin^{-1}(\lambda/2p)$, where λ is the wavelength of light and p is the pixel pitch. Clearly, the performance of the SLM cannot meet the needs of advanced applications such as near eye display. To increase the holographic FOV, the traditional way is to splice multiple SLMs^{11–13} or utilize curved holograms such as cylindrical diffractive optical elements^{14,15} and flexible materials.^{16,17} Graphene and meta-surfaces^{18–23} are also used to improve the performance of holograms.

Now, the concept of holography has been extended to nonlinear optics, leading to nonlinear holography.^{24–30} Compared to its linear counterpart, nonlinear holography reconstructs the images in the newly generated fields at second-, third-, and high-harmonic frequencies by spatially manipulating nonlinear coefficients, which has potential applications in optical storage and security encryption. One popular nonlinear hologram is lithium niobate (LN) with a

properly designed $\chi^{(2)}$ structure (i.e., nonlinear photonic crystal). One can modulate the amplitude or the sign of $\chi^{(2)}$ through amorphizing the LN crystalline^{30–33} or reversing the LN domain.^{34–39} Due to the limitation of traditional fabrication techniques, the pixel size of the LN nonlinear hologram is typically several micrometers in previous works, resulting in an FOV of several degrees.

Recently, we have developed a nonreciprocal femtosecond laser writing technique to fabricate LN nanodomains.³⁸ By using this technique, we experimentally demonstrate an ultra-high-resolution LN nonlinear hologram. The hologram pixel pitch reached 200 nm. In the experiment, the FOV of the second-harmonic (SH) field is extended to 120°. We demonstrate its applications in wide-view nonlinear holographic imaging, the generation of a two-dimensional (2D) SH spots array, and a high-numerical aperture (NA) SH cylindrical lens. Our method paves the way for the promotion of the performance of nonlinear holograms for high-end applications.

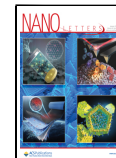
Figure 1a shows the experimental scheme of laser writing of LN domains. The light source is a mode-locked Ti:sapphire

Received: November 7, 2023

Revised: January 12, 2024

Accepted: January 12, 2024

Published: January 17, 2024



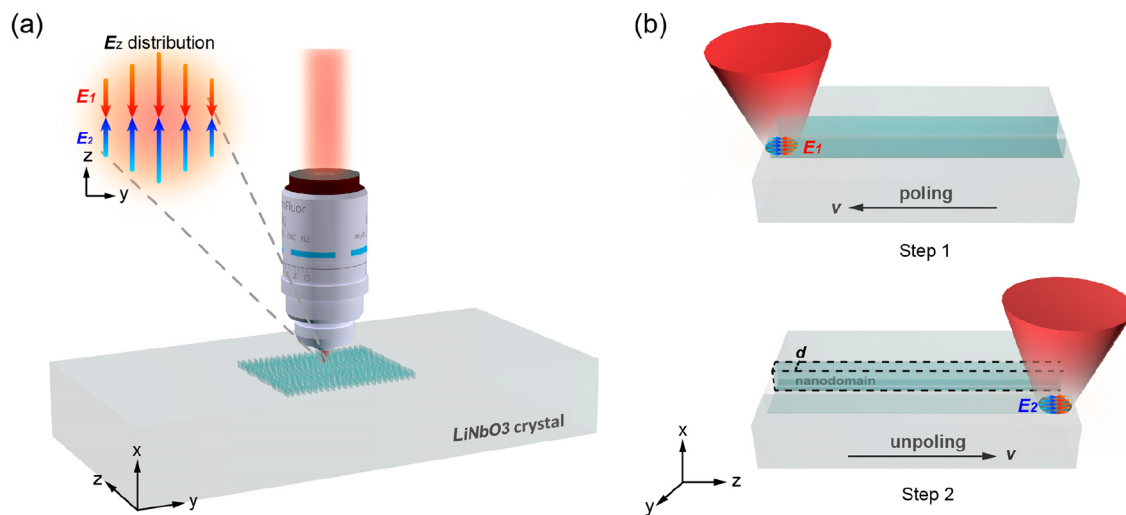


Figure 1. Nanofabrication of LN nonlinear holograms. (a) Schematic of the laser writing system. The hologram is fabricated in the y - z plane of the LN crystal. The inset shows the z -component of the laser-induced thermoelectric field through multiphoton absorption. (b) Typical process for fabricating LN nanodomains. In step 1, we move the laser beam along the $-z$ direction to write a domain line. In step 2, we shift the LN sample by a designed distance d along the y direction and then remove the partial domain by moving the laser beam back along the z direction. In this work, the minimal domain width (d) is 200 nm.

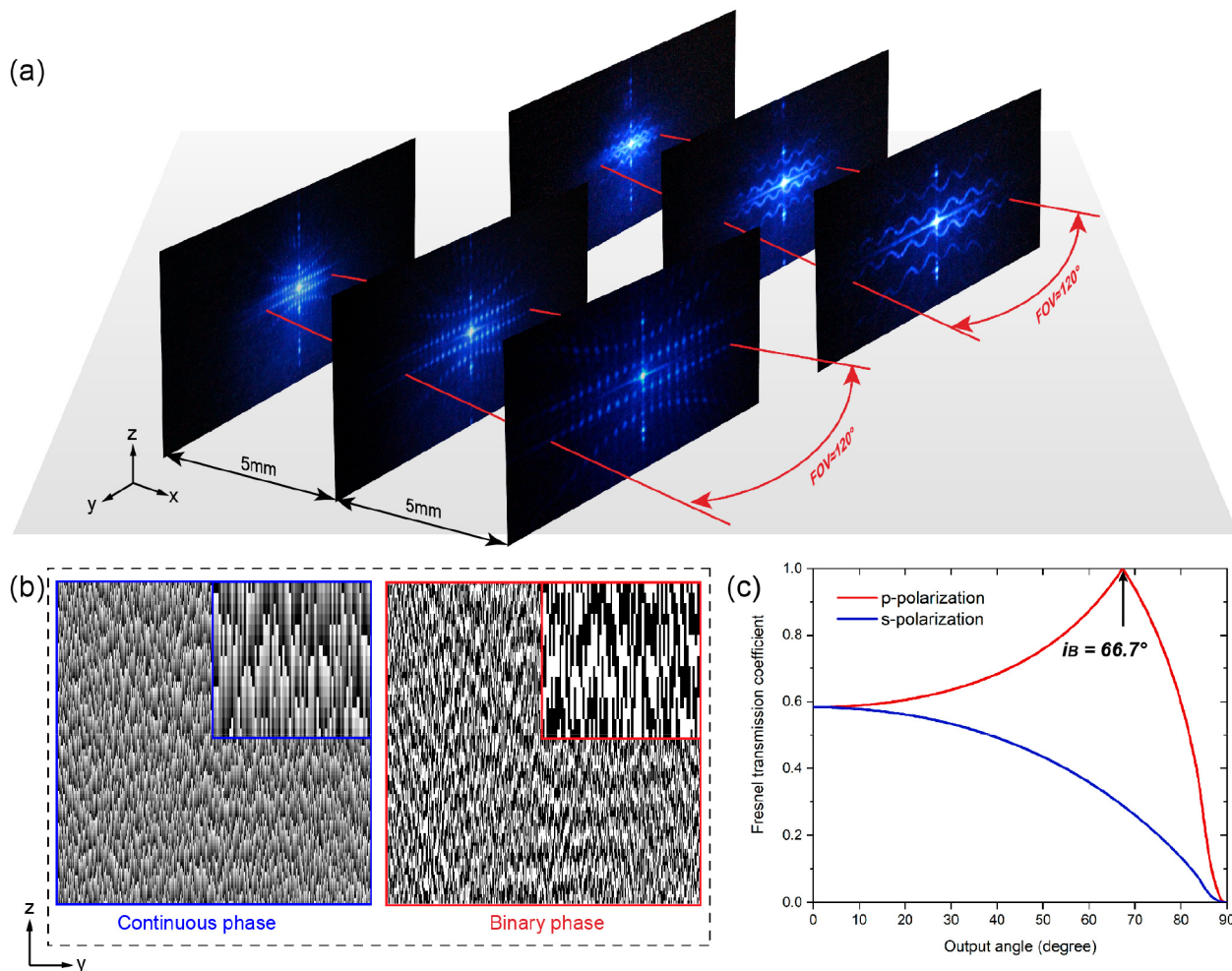


Figure 2. (a) Generation of SH dots and wavy lines. The fundamental wavelength is 800 nm. One can observe the SH pattern within an FOV of $\sim 120^\circ$. (b) Phase hologram for the generation of SH wavy lines calculated by using the G-S algorithm and then binarized to match the binary-phase modulation in the LN hologram. (c) Dependence of Fresnel transmission coefficients at an SH wavelength of 400 nm on the output angle from LN to air.

laser (Chameleon Vision-S, Coherent), which outputs short pulses at an 800 nm wavelength, a 75 fs pulse duration, and an 80 MHz repetition rate. The sample is 5% MgO-doped *x*-cut LN crystals. The linearly polarized laser beam is focused into the LN crystal by an oil immersion objective (63 \times , NA = 1.4). At the focal point of the laser beam, the spontaneous polarization of LN can be reversed due to the presence of a laser-induced thermoelectric field through multiphoton absorption. Notably, only the E_z component of the electric field is involved in the manipulation of the LN ferroelectric domain. E_z exhibits a head-to-head distribution (see the inset in Figure 1a), which results in the nonreciprocity of laser writing. Figure 1b shows a typical procedure for fabricating an LN nanodomain bypassing the diffraction limit of light. In the first step, the laser beam moves along the $-z$ direction. E_2 is applied first, which produces no domain structure because it is parallel to the spontaneous polarization of LN. Then, field E_1 that is antiparallel to the spontaneous polarization is applied, resulting in a reverted domain. In the second step, the laser beam moves along the $+z$ direction. The sequence of E_1 and E_2 being applied to LN is switched, which can be used to remove the existing domains partially or completely. In this way, we can fabricate a domain structure with a feature size beyond the diffraction limit of light. In experiment, we use a moving stage (P562.6CD, Physik Instrument) with a range of 200 μm (x) \times 200 μm (y) \times 200 μm (z) and an accuracy of 7 nm. The laser pulse energy is 2 nJ, the writing velocity 10 $\mu\text{m}/\text{s}$, and the typical time to fabricate one sample \sim 5 h.

The nonlinear hologram is designed by using the Gerchberg–Saxton (G-S) algorithm.⁴⁰ Considering that the SH waves generated in positive and negative LN domains have the same amplitude but a π -phase difference, we use the binary-phase nonlinear hologram for the experimental demonstration (Figure 2a). During the optimization process, we add a random phase into the target image as the initial input. After a certain number of iterations, one can obtain an optimized phase hologram. Then, we binarize the phase distribution (Figure 2b) to obtain the structure function of

$$H(y, z) = \begin{cases} 1, & H_{\text{GS}} > \pi \\ 0, & H_{\text{GS}} \leq \pi \end{cases} \quad (1)$$

where H_{GS} is the phase distribution directly calculated by the G-S algorithm. The distribution of $\chi^{(2)}$ in a nonlinear hologram is written as

$$\chi^{(2)}(y, z) = d_{\text{eff}}[2H(y, z) - 1] \quad (2)$$

where d_{eff} is the effective second-order nonlinear coefficient. In comparison to its linear counterpart, the design of an LN nonlinear hologram should consider the wavelength conversion and the binary-phase modulation.

Considering an SH generation process, the theoretical FOV of LN nonlinear hologram is decided by

$$\theta = 2 \sin^{-1}(\lambda_{2\omega}/2p) \quad (3)$$

where $\lambda_{2\omega}$ is the SH wavelength. In the experiment, we first test the FOV of a nonlinear hologram by reconstructing dots and wavy lines at the SH field. The nonlinear hologram (Figure 2b) is designed according to eqs 1 and 2. The hologram area is 100 μm (y) \times 100 μm (z), and the pixel size (p) 200 nm. The fundamental light with a wavelength of 800 nm is focused onto the LN hologram. Then, the transmitted fundamental light is filtered out by a short pass filter, and the far-field SH field is

projected on a screen. Figure 2a shows the recorded SH patterns at different distances. According to eq 3, one can achieve a full FOV of 180° in theory using a pixel size of 200 nm. However, the measured FOV in experiments is \sim 120°. We also fabricate a nonlinear grating for testing, and the SH diffraction can be observed within an FOV of \sim 143° (see Figure S1 for details). The difference is due to the low SH intensity at a large emit angle, resulting from the decreased transmissivity. We calculate the dependence of Fresnel transmission coefficients at the SH wavelength of 400 nm (Figure 2c). With an increase in the incident angle, the transmission coefficient of s-polarized light decreases monotonically while the transmission coefficient of p-polarized light reaches a peak and then decreases rapidly. In our experiment, we use a p-polarized fundamental wave, and the SH field gradually becomes indistinguishable at an output angle of $>$ 60°. At a pump power of 2.5 W, the conversion efficiencies are 1.7×10^{-5} and 8×10^{-7} for s- and p-polarized fundamental light, respectively. In addition, the SH pattern is distorted at a large angle, which can be attributed to the invalidation of paraxial approximation (see Figure S2 for details).

To suppress the image distortion, we add an objective (50 \times , NA = 0.8) right after the nonlinear hologram (Figure S3). Its function is to perform Fourier transform of the SH field in the hologram plane. The cost is that the NA value of the used objective defines the range of the collected SH field. In experiments, we reconstruct the 2D projections of a series of cubes from different view angles at SH fields. The total FOV is designed to be 90°. The fundamental wavelength is set at 800 nm. The simulated SH pattern at 400 nm is shown in Figure 3a, in which four cubes are present at view angles of -45° , -15° , 15° , and 45° . The experimental patterns with negligible distortions are quite consistent with the numerical simulations. In addition, by properly designing the nonlinear hologram, one can combine multiple diffraction orders of SH lights together to extend the holographic field. In experiments, we use this strategy to demonstrate the generation of a hexagonal SH

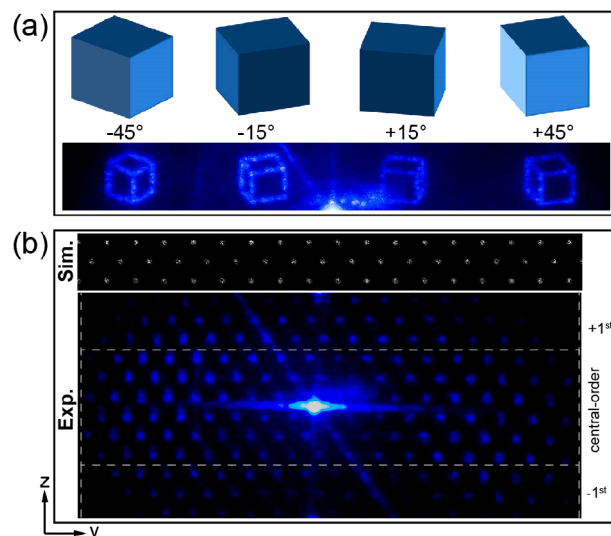


Figure 3. After Fourier transform through an objective, one can reconstruct SH images with negligible distortions. (a) Reconstruction of a cube with different view angles (-45° , -15° , 15° , and 45°) at the SH field. (b) By properly designing the nonlinear hologram, one can combine the central and first and higher orders of SH fields to compose a large-area hexagonal array.

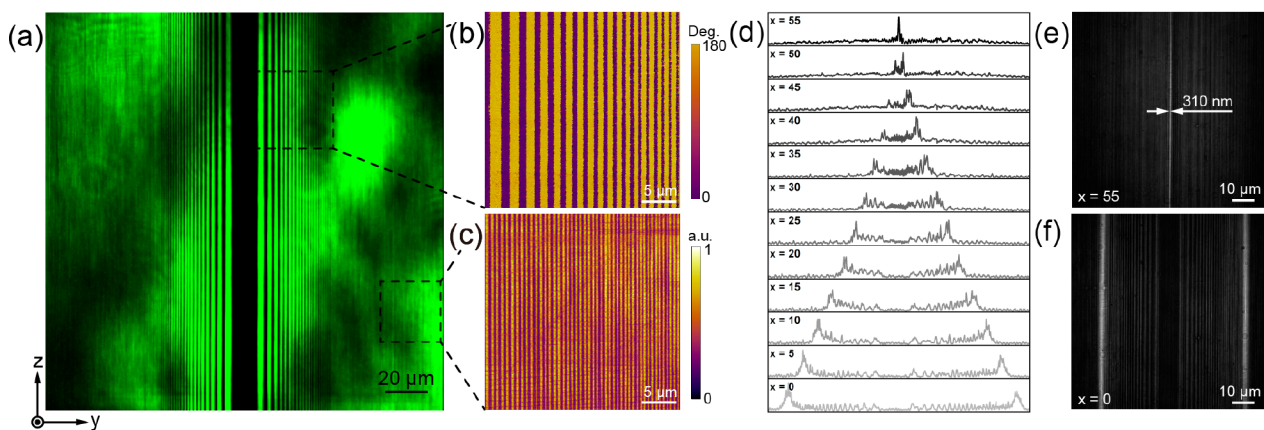


Figure 4. Demonstration of a nonlinear cylindrical lens. (a) Optical image of a nonlinear cylindrical lens recorded by confocal SH microscopy. The details are measured by using lateral piezoresponse force microscopy (PFM) as shown in panels b and c. (d) Normalized SH intensity profiles at different distances from the sample. One can clearly observe the tight focusing of SH light. (e and f) SH patterns at $x = 0 \mu\text{m}$ (i.e., the sample surface) and $x = 55 \mu\text{m}$ (i.e., the focal plane), respectively.

array. As shown in Figure 3b, a uniform SH array is reconstructed by combining the central and first and higher orders of the SH lights. The FOV is measured to be 106° along the y direction. The array parameters, including its period and symmetry, can be easily tuned by optimizing the nonlinear hologram.

In addition, the nonlinear hologram with a subwavelength pixel size can be used as a high-NA lens working at the SH wavelength. Here, we design a nonlinear cylindrical lens as an example. The phase distribution of a cylindrical lens in the $y-z$ plane is written as

$$H_{\text{CL}} = \frac{2\omega}{c} \left(\sqrt{f^2 + y^2} - f \right) \quad (4)$$

where ω is the frequency of the fundamental wave and f is the focal length. By binarizing phase distribution H_{CL} , we obtain the structure function of a nonlinear hologram, i.e.

$$H(y, z) = \begin{cases} 1, & H_{\text{CL}} > \pi \\ 0, & H_{\text{CL}} \leq \pi \end{cases} \quad (5)$$

Figure 4a shows an image of the used nonlinear cylindrical lens, which consists of striped domains with designed widths. The structure area is $190 \mu\text{m}$ (y) \times $190 \mu\text{m}$ (z), and the domain line width decreases gradually from $2 \mu\text{m}$ to 200 nm . Panels b and c of Figure 4 show the lateral PFM phase and amplitude images, respectively, which present the details of a nonlinear cylindrical lens. In the experiment, we input an 800 nm laser beam along the x direction. The SH intensity profiles at different propagation distances are listed in Figure 4d. Measured focal length f is $55 \mu\text{m}$, which is consistent with the designed value. Correspondingly, the NA of the nonlinear cylindrical lens reaches 0.86. Panels e and f of Figure 4 show the recorded SH patterns at x values of 0 and $55 \mu\text{m}$, respectively. The full width at half-maximum of the focused line in Figure 4e is measured to be 310 nm . The theoretical value⁴¹ is calculated to be $\lambda_{2\omega}/(2 \times \text{NA}) \approx 233 \text{ nm}$. The difference can be explained by the reduced transmissivity of light with a high spatial frequency.

To summarize, we have proposed and experimentally investigated an ultra-high-resolution nonlinear hologram in the LN crystal. Using the femtosecond laser poling technique, the pixel size is reduced to 200 nm . Correspondingly, the FOV

of the generated harmonic field is extended beyond 120° in experiments. In addition, we demonstrate its applications in large FOV nonlinear holography, generation of a high-density SH spot array, and a high-NA cylindrical lens working at the SH wavelength. Under our experimental configuration, the FOV of the output SH field is ultimately limited by Fresnel transmission coefficients. There are several potential ways to further improve the performance of the LN hologram. For example, advanced algorithms without paraxial approximation are required to remove the image distortions at large angles.^{42,43} A curved LN hologram helps suppress the negative effect of the Fresnel transmittance. The signal-to-noise ratio of the generated SH image can be improved by using a thin LN crystal to reduce the background noise or optimizing the laser writing parameters to reduce the scattering loss. Also, one may use LN nanodomains to compose a superpixel hologram for complex-amplitude modulation of nonlinear waves for high-quality imaging. Our method provides a powerful platform for manipulating nonlinear optical interactions for advanced applications across different wavelength bands.

ASSOCIATED CONTENT

Supporting Information

The Supporting Information is available free of charge at <https://pubs.acs.org/doi/10.1021/acs.nanolett.3c04286>.

SH diffraction pattern of a nonlinear grating (Figure S1), image distortion at large emit angles (Figure S2), and schematic illustration of the experimental setup for nonlinear holography (Figure S3) (PDF)

AUTHOR INFORMATION

Corresponding Author

Yong Zhang — National Laboratory of Solid State Microstructures, College of Engineering and Applied Sciences, School of Physics, and Collaborative Innovation Center of Advanced Microstructures, Nanjing University, Nanjing 210093, China; orcid.org/0000-0003-1158-2248; Email: zhangyong@nju.edu.cn

Authors

Xiaoyi Xu — National Laboratory of Solid State Microstructures, College of Engineering and Applied Sciences,

School of Physics, and Collaborative Innovation Center of Advanced Microstructures, Nanjing University, Nanjing 210093, China

Pengcheng Chen — National Laboratory of Solid State Microstructures, College of Engineering and Applied Sciences, School of Physics, and Collaborative Innovation Center of Advanced Microstructures, Nanjing University, Nanjing 210093, China

Taxue Ma — National Laboratory of Solid State Microstructures, College of Engineering and Applied Sciences, School of Physics, and Collaborative Innovation Center of Advanced Microstructures, Nanjing University, Nanjing 210093, China

Jianan Ma — National Laboratory of Solid State Microstructures, College of Engineering and Applied Sciences, School of Physics, and Collaborative Innovation Center of Advanced Microstructures, Nanjing University, Nanjing 210093, China

Chao Zhou — National Laboratory of Solid State Microstructures, College of Engineering and Applied Sciences, School of Physics, and Collaborative Innovation Center of Advanced Microstructures, Nanjing University, Nanjing 210093, China

Yawen Su — National Laboratory of Solid State Microstructures, College of Engineering and Applied Sciences, School of Physics, and Collaborative Innovation Center of Advanced Microstructures, Nanjing University, Nanjing 210093, China

Mingxin Lv — National Laboratory of Solid State Microstructures, College of Engineering and Applied Sciences, School of Physics, and Collaborative Innovation Center of Advanced Microstructures, Nanjing University, Nanjing 210093, China

Weiwen Fan — National Laboratory of Solid State Microstructures, College of Engineering and Applied Sciences, School of Physics, and Collaborative Innovation Center of Advanced Microstructures, Nanjing University, Nanjing 210093, China

Bohan Zhai — National Laboratory of Solid State Microstructures, College of Engineering and Applied Sciences, School of Physics, and Collaborative Innovation Center of Advanced Microstructures, Nanjing University, Nanjing 210093, China

Yuyang Sun — National Laboratory of Solid State Microstructures, College of Engineering and Applied Sciences, School of Physics, and Collaborative Innovation Center of Advanced Microstructures, Nanjing University, Nanjing 210093, China

Tianxin Wang — National Laboratory of Solid State Microstructures, College of Engineering and Applied Sciences, School of Physics, and Collaborative Innovation Center of Advanced Microstructures, Nanjing University, Nanjing 210093, China

Xiaopeng Hu — National Laboratory of Solid State Microstructures, College of Engineering and Applied Sciences, School of Physics, and Collaborative Innovation Center of Advanced Microstructures, Nanjing University, Nanjing 210093, China

Shi-Ning Zhu — National Laboratory of Solid State Microstructures, College of Engineering and Applied Sciences, School of Physics, and Collaborative Innovation Center of Advanced Microstructures, Nanjing University, Nanjing 210093, China

Min Xiao — National Laboratory of Solid State Microstructures, College of Engineering and Applied Sciences, School of Physics, and Collaborative Innovation Center of Advanced Microstructures, Nanjing University, Nanjing 210093, China; Department of Physics, University of Arkansas, Fayetteville, Arkansas 72701, United States

Complete contact information is available at:
<https://pubs.acs.org/10.1021/acs.nanolett.3c04286>

Author Contributions

[§]X.X., P.C., and T.M. contributed equally to this work.

Funding

This work was supported by the National Key R&D Program of China (2022YFA1205100), the National Natural Science Foundation of China (NSFC) (91950206, 12174185, 92150302, and 92163216), the China Postdoctoral Science Foundation (2023M731587 and 2023T160303), the Jiangsu Funding Program for Excellent Postdoctoral Talent (2023ZB632), the Youth Foundation of Jiangsu Province (BK20230768), the Yuxiu Young Scholars Program of Nanjing University, and the Fundamental Research Funds for the Central Universities (021314380226).

Notes

The authors declare no competing financial interest.

REFERENCES

- (1) Heaney, J. F.; Bashaw, M. C.; Hesselink, L. Volume holographic storage and retrieval of digital data. *Science* **1994**, *265*, 749–752.
- (2) Hesselink, L.; Orlov, S. S.; Liu, A.; Akella, A.; Lande, D.; Neurgaonkar, R. R. Photorefractive materials for nonvolatile volume holographic data storage. *Science* **1998**, *282*, 1089–1094.
- (3) Georgi, P.; Wei, Q.; Sain, B.; Schlickriede, C.; Wang, Y.; Huang, L.; Zentgraf, T. Optical secret sharing with cascaded metasurface holography. *Sci. Adv.* **2021**, *7* (16), eabf9718.
- (4) Zhao, R.; Sain, B.; Wei, Q.; Tang, C.; Li, X.; Weiss, T.; Huang, L.; Wang, Y.; Zentgraf, T. Multichannel vectorial holographic display and encryption. *Light: Sci. Appl.* **2018**, *7* (1), 95.
- (5) Hou, J.; Situ, G. Image encryption using spatial nonlinear optics. *eLight* **2022**, *2* (1), 3.
- (6) Kim, M. K. Principles and techniques of digital holographic microscopy. *J. Photonics Energy* **2010**, *018005*.
- (7) Gabor, D. A new microscopic principle. *Nature* **1948**, *161*, 777–778.
- (8) Brown, B. R.; Lohmann, A. W. Complex spatial filtering with binary masks. *Appl. Opt.* **1966**, *5* (6), 967–969.
- (9) Slinger, C.; Cameron, C.; Stanley, M. Computer-generated holography as a generic display technology. *Computer* **2005**, *38* (8), 46–53.
- (10) Xiong, J.; Wu, S.-T. Planar liquid crystal polarization optics for augmented reality and virtual reality: from fundamentals to applications. *eLight* **2021**, *1* (1), 3.
- (11) Hahn, J.; Kim, H.; Lim, Y.; Park, G.; Lee, B. Wide viewing angle dynamic holographic stereogram with a curved array of spatial light modulators. *Opt. Express* **2008**, *16* (16), 12372.
- (12) Yaras, F.; Kang, H.; Onural, L. Circular holographic video display system. *Opt. Express* **2011**, *19* (10), 9147–9156.
- (13) Liu, S. J.; Wang, D.; Zhai, F. X.; Liu, N. N.; Hao, Q. Y. Holographic display method with a large field of view based on a holographic functional screen. *Appl. Opt.* **2020**, *59* (20), 5983–5988.
- (14) Ma, Y.; Wang, J.; Wu, Y.; Jin, F.; Zhang, Z.; Zhou, Z.; Chen, N. Large field-of-view holographic display by gapless splicing of multisegment cylindrical holograms. *Appl. Opt.* **2021**, *60* (24), 7381–7390.
- (15) Goncharsky, A.; Durlevich, S. Cylindrical computer-generated hologram for displaying 3D images. *Opt. Express* **2018**, *26* (17), 22160–22167.

- (16) Xue, G. L.; Zhang, Q. M.; Liu, J.; Wang, Y. T.; Gu, M. Flexible holographic 3D display with wide viewing angle. *Frontiers in Optics* **2016**, *3*.
- (17) Malek, S. C.; Ee, H.-S.; Agarwal, R. Strain Multiplexed Metasurface Holograms on a Stretchable Substrate. *Nano Lett.* **2017**, *17* (6), 3641–3645.
- (18) Li, X.; Ren, H.; Chen, X.; Liu, J.; Li, Q.; Li, C.; Xue, G.; Jia, J.; Cao, L.; Sahu, A.; Hu, B.; Wang, Y.; Jin, G.; Gu, M. Athermally photoreduced graphene oxides for three-dimensional holographic images. *Nat. Commun.* **2015**, *6*, 6984.
- (19) Chen, J.; Ye, X.; Gao, S.; Chen, Y.; Zhao, Y.; Huang, C.; Qiu, K.; Zhu, S.; Li, T. Planar wide-angle-imaging camera enabled by metalens array. *Optica* **2022**, *9* (4), 431–437.
- (20) Huang, L.; Chen, X.; Mühlenernd, H.; Zhang, H.; Chen, S.; Bai, B.; Tan, Q.; Jin, G.; Cheah, K.-W.; Qiu, C.-W.; Li, J.; Zentgraf, T.; Zhang, S. Three-dimensional optical holography using a plasmonic metasurface. *Nat. Commun.* **2013**, *4* (1), 2808.
- (21) Ni, Y.; Chen, S.; Wang, Y.; Tan, Q.; Xiao, S.; Yang, Y. Metasurface for Structured Light Projection over 120 degrees Field of View. *Nano Lett.* **2020**, *20* (9), 6719–6724.
- (22) Yue, Z.; Xue, G.; Liu, J.; Wang, Y.; Gu, M. Nanometric holograms based on a topological insulator material. *Nat. Commun.* **2017**, *8*, 15354.
- (23) Zheng, G.; Mühlenernd, H.; Kenney, M.; Li, G.; Zentgraf, T.; Zhang, S. Metasurface holograms reaching 80% efficiency. *Nat. Nanotechnol.* **2015**, *10* (4), 308–312.
- (24) Ye, W.; Zeuner, F.; Li, X.; Reineke, B.; He, S.; Qiu, C. W.; Liu, J.; Wang, Y.; Zhang, S.; Zentgraf, T. Spin and wavelength multiplexed nonlinear metasurface holography. *Nat. Commun.* **2016**, *7*, 11930.
- (25) Gao, Y.; Fan, Y.; Wang, Y.; Yang, W.; Song, Q.; Xiao, S. Nonlinear Holographic All-Dielectric Metasurfaces. *Nano Lett.* **2018**, *18* (12), 8054–8061.
- (26) Almeida, E.; Bitton, O.; Prior, Y. Nonlinear metamaterials for holography. *Nat. Commun.* **2016**, *7*, 12533.
- (27) Liu, S.; Mazur, L. M.; Krolkowski, W.; Sheng, Y. Nonlinear Volume Holography in 3D Nonlinear Photonic Crystals. *Laser Photonics Rev.* **2020**, *14* (11), 2000224.
- (28) Fang, X.; Wang, H.; Yang, H.; Ye, Z.; Wang, Y.; Zhang, Y.; Hu, X.; Zhu, S.; Xiao, M. Multichannel nonlinear holography in a two-dimensional nonlinear photonic crystal. *Phys. Rev. A* **2020**, *102* (4), 043506.
- (29) Dasgupta, A.; Gao, J.; Yang, X. Atomically Thin Nonlinear Transition Metal Dichalcogenide Holograms. *Nano Lett.* **2019**, *19* (9), 6511–6516.
- (30) Chen, P.; Wang, C.; Wei, D.; Hu, Y.; Xu, X.; Li, J.; Wu, D.; Ma, J.; Ji, S.; Zhang, L.; Xu, L.; Wang, T.; Xu, C.; Chu, J.; Zhu, S.; Xiao, M.; Zhang, Y. Quasi-phase-matching-division multiplexing holography in a three-dimensional nonlinear photonic crystal. *Light: Sci. Appl.* **2021**, *10* (1), 146.
- (31) Wei, D. Z.; Wang, C. W.; Wang, H. J.; Hu, X. P.; Wei, D.; Fang, X. Y.; Zhang, Y.; Wu, D.; Hue, Y. L.; Li, J. W.; Zhu, S. N.; Xiao, M. Experimental demonstration of a three-dimensional lithium niobate nonlinear photonic crystal. *Nat. Photonics* **2018**, *12* (10), 596–601.
- (32) Wei, D. Z.; Wang, C. W.; Xu, X. X.; Wang, H. J.; Hu, Y. L.; Chen, P. C.; Li, J. W.; Zhu, Y. Z.; Xin, C.; Hu, X. P.; Zhang, Y.; Wu, D.; Chu, J. R.; Zhu, S. N.; Xiao, M. Efficient nonlinear beam shaping in three-dimensional lithium niobate nonlinear photonic crystals. *Nat. Commun.* **2019**, *10* (1), 4193.
- (33) Zhu, B.; Liu, H.; Liu, Y.; Yan, X.; Chen, Y.; Chen, X. Second-harmonic computer-generated holographic imaging through monolithic lithium niobate crystal by femtosecond laser micromachining. *Opt. Lett.* **2020**, *45* (15), 4132–4135.
- (34) Hong, X. H.; Yang, B.; Zhang, C.; Qin, Y. Q.; Zhu, Y. Y. Nonlinear volume holography for wave-front engineering. *Phys. Rev. Lett.* **2014**, *113* (16), 163902.
- (35) Lu, R.; Zhao, R.; Feng, X.; Zhang, C.; Hong, X.; Qin, Y.; Zhu, Y. Nonlinear Wavefront Shaping and Imaging in Nonlinear Photonic Crystals with a Generalized Quasi-Multivalue-Encoding Method. *ACS Photon.* **2021**, *8* (11), 3133–3140.
- (36) Shapira, A.; Shiloh, R.; Juwiler, I.; Arie, A. Two-dimensional nonlinear beam shaping. *Opt. Lett.* **2012**, *37* (11), 2136–2138.
- (37) Chen, P.; Xu, X.; Wang, T.; Zhou, C.; Wei, D.; Ma, J.; Guo, J.; Cui, X.; Cheng, X.; Xie, C.; Zhang, S.; Zhu, S.; Xiao, M.; Zhang, Y. Laser nanoprinting of 3D nonlinear holograms beyond 25000 pixels-per-inch for inter-wavelength-band information processing. *Nat. Commun.* **2023**, *14* (1), 5523.
- (38) Xu, X.; Wang, T.; Chen, P.; Zhou, C.; Ma, J.; Wei, D.; Wang, H.; Niu, B.; Fang, X.; Wu, D.; Zhu, S.; Gu, M.; Xiao, M.; Zhang, Y. Femtosecond laser writing of lithium niobate ferroelectric nanodomains. *Nature* **2022**, *609* (7927), 496–501.
- (39) Imbrock, J.; Hanafi, H.; Ayoub, M.; Denz, C. Local domain inversion in MgO-doped lithium niobate by pyroelectric field-assisted femtosecond laser lithography. *Appl. Phys. Lett.* **2018**, *113* (25), 252901.
- (40) Gerchberg, R.; Saxton, W. O. A practical algorithm for the determination of plane from image and diffraction pictures. *Optik* **1972**, *35* (2), 237–246.
- (41) Khorasaninejad, M.; Chen, W. T.; Devlin, R. C.; Oh, J.; Zhu, A. Y.; Capasso, F. Metaleenses at visible wavelengths: Diffraction-limited focusing and subwavelength resolution imaging. *Science* **2016**, *352* (6290), 1190–1194.
- (42) Szpygiel, J.; Chlipala, M.; Kukolowicz, R.; Idicula, M.; Kozacki, T. Distortion correction for wide angle holographic projector. *Photonics Letters of Poland* **2021**, *13* (4), 79–81.
- (43) Nguyen, G.-N.; Heggarty, K.; Bacher, A.; Jakobs, P.-J.; Häringer, D.; Gérard, P.; Pfeiffer, P.; Meyrueis, P. Iterative scalar nonparaxial algorithm for the design of Fourier phase elements. *Opt. Lett.* **2014**, *39* (19), 5551–5554.

Recommended by ACS

Asymmetric Full-Color Vectorial Meta-holograms Empowered by Pairs of Exceptional Points

Zijin Yang, Qinghua Song, et al.

JANUARY 08, 2024

NANO LETTERS

READ

Object Function Retrieval by Model-Based Optimization in Fourier Holographic Endoscopy

Thi Van Anh Nguyen, Wonshik Choi, et al.

JANUARY 08, 2024

ACS PHOTONICS

READ

Switchable Two-Dimensional AND and Exclusive OR Operation Based on Dual-Wavelength Metasurfaces

Chang Peng, Guoxing Zheng, et al.

JANUARY 26, 2024

ACS NANO

READ

Achromatic Imaging Systems with Flat Lenses Enabled by Deep Learning

Roy Maman, Uriel Levy, et al.

DECEMBER 11, 2023

ACS PHOTONICS

READ

Get More Suggestions >